PHYSICAL REVIEW B VOLUME 10, NUMBER 7 1 OCTOBER 1974

Feynman-graph theory of the Kondo effect. II. Self-consistent clothing of parquet graphs*†

W. S. Verwoerd
Department of Physics, University of Pretoria, Pretoria, Republic of South Africa
(Received 11 September 1973)

The calculation of the resistivity R of a Kondo system with a $S=1/2$ impurity in the previous paper is extended to include also parquet graphs with self-consistently-clothed conduction-electron propagators. The formalism used preserves a close contact with the non-self-consistent treatment, and can be used to understand the radical difference betweeen the results. The main result of this paper is a numerical relation between the normalized resistivity R/R_u and $\ln(T/T_K)$, where R_u is the unitarity limit and T_K the Kondo temperature. A comparison with experimental values and with the Hamann formula is carried out. Our results fit the data better at high temperatures, but neither theory saturates fast enough to R_u as the temperature approaches zero. Finally it is shown by which approximations Hamann's integral equation can be derived from our self-consistent equations.

I. INTRODUCTION

In the previous paper[1] (hereafter referred to as paper I) the self-energy of a conduction-electron exchange interacting with a single $S=\frac{1}{2}$ impurity atom was calculated by an improved summation of ordinary parquet graphs. From this the Kondo contribution to the resistivity R was calculated. The divergence at the Kondo temperature occurring in previous work was found to be replaced by a smooth maximum, but at $T=0$ the resistivity still approached zero. It is well known that this is unphysical and that R should instead saturate at the unitarity limit value R_u.

In paper I it was shown that the non-self-consistent form of the Nagaoka[2] decoupled equation-of-motion theory leads to an expression for R which is an approximation to our parquet-sum expression. Nevertheless, in its self-consistent form, the Nagaoka-Hamann-Bloomfield theory[2-4] yields the required saturation at low temperatures. Essentially the same result is also obtained by Cheung and Mattuck[5] in a self-consistent perturbation-theory calculation.

In this paper we therefore address ourselves to the task of finding the Kondo resistivity by including also the clothed or self-consistent parquet graphs in our self-energy calculation. Section II is devoted to the derivation of a series of self-consistent equations which connect the self-energy Σ to the pair bubble or s functions,[1] the s functions to the T matrix, and the T matrix to the self-energy.

Approximating $T\simeq\Sigma$, we solve these equations in Sec. III for the s functions evaluated at the Fermi surface. Our final result is a numerical relation between R and $\ln(T/T_K)$ where T_K is the Kondo temperature defined in paper I. Saturation to R_u at $T=0$ is obtained, as illustrated in Fig. 5, and numerical values are given in Table I. Qualitatively there is a close resemblance between our results and the Hamann formula [Eq. (4.1)]. When drawn as functions of $\ln(T/T_K)$, both represent rounded off step functions having a width of about 6 decades in the temperature (compared to a typical experimental width of 1–3 decades).

Section IV discusses the fitting of both theoretical results to experimental data for CuCr. We find (see Fig. 6) that our theory gives a better fit than the Hamann formula in the high-temperature region, but because of the discrepancy between theoretical and experimental widths neither theory can reproduce the fast rise to the unitarity limit below T_K.

Apart from the improved fit, our treatment has the advantage that a close contact between the ordinary and self-consistent versions of the theory is maintained. As a result, added insight is gained into the perhaps puzzling question why self-consistency drastically alters the behavior of the system at zero temperature, although the self-consistent terms are of lesser order in the logarithmic divergence and could be expected to be of importance only near the Kondo temperature. This matter is investigated in Sec. III.

It was stated in paper I that one purpose of our work is to develop a systematic perturbation theory of the Kondo effect which can serve as a basis of comparison with pure Kondo model calculations. The numerical comparison with the Nagaoka-Hamann-Bloomfield theory is supplemented in Appendix A by a derivation of Hamann's integral equation from our self-consistent equations. The approximations made in the process lead us to suspect that the Nagaoka decoupling implies a low-interaction strength J, and that the T matrix obtained from Hamann's equation is accurate only on the Fermi surface.

TABLE I. Normalized resistivity as a function of normalized temperature.

T/T_K	R/R_u	T/T_K	R/R_u
1000	0.0900	0.9	0.7460
600	0.1029	0.8	0.7585
300	0.1248	0.7	0.7719
100	0.1754	0.6	0.7866
80	0.1896	0.5	0.8028
60	0.2085	0.4	0.8209
40	0.2408	0.3	0.8419
20	0.3108	0.2	0.8672
10	0.4015	0.1	0.9011
9	0.4169	0.09	0.9054
8	0.4344	0.07	0.9148
7	0.4548	0.045	0.9289
6	0.4788	0.03	0.9396
5	0.5074	0.02	0.9486
4	0.5425	0.01	0.9605
3	0.5870	0.006	0.9673
2	0.6465	0.003	0.9745
1	0.7345	0.001	0.9823

II. SELF-CONSISTENT RELATIONS BETWEEN Σ, s, AND T

Self-energy in terms of s functions. The expansion of the self-energy Σ in a series of parquet diagrams is discussed in detail in paper I, Sec. III, where various terms used here are defined.

The summation performed in paper I included only the ordinary parquet graph contributions to the self-energy. It can be seen that all the self-consistent parquet graphs (simple examples of which are given in the last line of Fig. 3 of paper I) can be included in the sum by clothing the conduction electron (k-electron) propagators in each ordinary parquet graph with the ordinary parquet graph self-energy. This means that we must repeat the summation of ordinary parquet graphs, but with the k-electron propagators (solid lines) reinterpreted as the interacting Green's function $\mathcal{G}$ instead of the unperturbed Green's function $\mathcal{G}_0$.

As a first example, consider the simplest parquet graph, Σ_1 of Fig. 1. Note that we leave the localized or d-electron propagators (broken lines) bare as explained in paper I, Sec. IIIB. Using the conventions of Ref. 6 and 7, Fig. 1 is translated into an algebraic form. We use the same notation as in paper I, e.g., k, k', p and q are used to label conduction-electron momentum states with energy ϵ_k, etc., all measured from the Fermi level (i.e., $\epsilon_F = 0$). The two localized states are represented by $d\uparrow$ and $d\downarrow$, having opposite spin projections and energies (adjusted by Lagrange multipliers) of $\pm U$, respectively. It is then found that

$$\Sigma_1 = -(4J^2/\beta)\sum_{n2}(i\omega_{n2} - U)^{-1} s(i\omega_n + i\omega_{n2}), \qquad (2.1)$$

where the interaction strength of the Kondo interaction[8] $J(\text{Kondo}) = 2NJ$, and

$$s(i\omega_n + i\omega_{n2}) = \beta^{-1} \sum_{p,q,m1} \mathcal{G}_0(d\uparrow;\ \omega_{n2} - \gamma_{m1}) \times \mathcal{G}(p, q;\ \omega_n + \gamma_{m1}), \qquad (2.2)$$

$$\omega_n = (2n+1)\pi\beta^{-1} \text{ and } \gamma_m = 2m\pi\beta^{-1}. \qquad (2.3)$$

The summation over $m1$ in Eq. (2.2) can be performed by writing $\mathcal{G}$ in its Lehmann representation

$$\mathcal{G}(p, q;\ \omega_n) = \int_{-\infty}^{\infty} d\omega' A(p, q, \omega')(i\omega_n - \omega')^{-1}, \qquad (2.4)$$

$$A(p, q;\omega) = -\pi^{-1}\,\mathrm{Im}\,\mathcal{G}(p, q;\ \omega + i\delta). \qquad (2.5)$$

Substituting Eq. (2.4) into Eq. (2.2) and performing the sum, we find

$$s(i\omega_n + i\omega_{n2}) = \int d\omega' \sum_{p,q} A(p, q;\ \omega')[f(\omega') - f(U)] \times (i\omega_n + i\omega_{n2} - \omega' + U)^{-1}, \qquad (2.6)$$

where $f(z)$ is defined by

$$f(z) = (1 + e^{\beta z})^{-1}. \qquad (2.7)$$

When the spectral function $A_0(p, q;\omega') = \delta(\omega' - \epsilon_p)\delta_{pq}$ of the unperturbed Green's function is substituted in Eq. (2.6), Eq. (2.1) is reduced to its bare propagator counterpart, Eq. (4.2) of paper I. This shows that s is simply the clothed version of the bare propagator s functions used in paper I.

As made clear in paper I (sec. IIB) we make use of the s function in the two opposite limits of a pure $S = \uparrow$ or $S = \downarrow$ state for the unperturbed spin state of the impurity atom relative to the spin of the entering k line. These s functions are denoted by $s_\uparrow$ and $s_\downarrow$, respectively, and found by letting $U \to \pm 0$ except that wherever the temperature dependent statistical factor $e^{\beta U}$ appears, the limit $\beta \to \infty$ is taken in such a way that $|\beta U| \to \infty$ [see Eq. (4.4) of paper I]. The result is

$$s_\uparrow(i\omega_n) = \int d\omega' \sum_{p,q} A(p, q;\omega') f(\omega') \times (i\omega_n - \omega')^{-1}, \qquad (2.8)$$

$$s_\downarrow(i\omega_n) = \int d\omega' \sum_{p,q} A(p, q;\omega')[f(\omega') - 1] \times (i\omega_n - \omega')^{-1}. \qquad (2.9)$$

Substituting A_0 for A reduces Eqs. (2.8) and (2.9) to the definitions of the corresponding bare s functions, Eqs. (4.5) and (4.6) of paper I. Moreover, comparison of Eqs. (2.8) and (2.9) with their bare counterparts shows that the clothed s functions depend on their arguments in a similar way as the bare s functions. Consequently, Poisson summations over the arguments of s functions can be performed in the same way for both cases, and the results obtained in paper I for the various contribu-

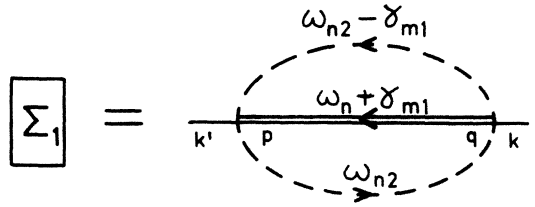

FIG. 1. Self-consistent clothing in a simple parquet graph.

tions to the self-energy Σ in terms of s functions are found to remain valid when these are reinterpreted as clothed functions. A simple example is Σ_1 in Eq. (2.1), which can be reduced with the help of Eq. (2.8) to the same form as Eq. (4.5) of paper I.

In particular, the parquet-sum self-energy is again given by [compare Eq. (3.22) of paper I]

$$\Sigma_{\uparrow,\downarrow}=\mp[J-4J^2 s_{\uparrow,\downarrow}(1+2Js_{\uparrow,\downarrow})^{-1}]. \tag{2.10}$$

The s functions in terms of self-energy. The interacting propagator can be expressed in terms of noninteracting propagators and the single-particle transition or T matrix as indicated in Fig. 2. As is clear from the figure, the T matrix is interpreted diagrammatically as the reducible self-energy, i.e.,

$$T(\omega_n)=\Sigma(\omega_n)\left(1-\Sigma(\omega_n)\sum_p \mathcal{G}_0(p,\omega_n)\right)^{-1}. \tag{2.11}$$

This equation applies for both $S=\uparrow$ and $S=\downarrow$ subscripts, but one must be careful which of $T_\uparrow$ and $T_\downarrow$ is used to clothe the intermediate k line. When considering $s_\uparrow$, for example, the unperturbed impurity spin is parallel to the spin of the incoming k line (which, per definition, has spin up). Throughout I the approximation is used that all intermediate k lines are on the same side of the Fermi surface (see Secs. III B, III C, and IV C of paper I) which also implies that they all have spin down. In other words, the reference direction in intermediate states is reversed and the intermediate k line in $s_\uparrow$ must be clothed with $T_\downarrow$ and vice versa.[9]

According to Eq. (2.5) the unknown sum of spectral amplitudes A in Eq. (2.8) is related to the following sum of Green's functions, evaluated from Fig 2:

$$\sum_{p,q}\mathcal{G}(p,q;\omega+i\delta)=\sum_p \mathcal{G}_0(p;\omega+i\delta)+T_\downarrow(\omega+i\delta)\sum_p \mathcal{G}_0(p;\omega+i\delta)\times\sum_q \mathcal{G}_0(q;\omega+i\delta). \tag{2.12}$$

The sum of unperturbed Green's functions can be evaluated as an integral over energies, weighted by a square density of states with value ρ in a region of width $2D$ centered at the Fermi level, and zero elsewhere. We find

$$\sum_p \mathcal{G}_0(p;\omega+i\delta)\simeq i\pi\rho. \tag{2.13}$$

In Eq. (2.13) we have neglected the real part of the sum, which is zero at the Fermi level ($\omega=0$) and varies slowly elsewhere. This approximation was also used by previous authors and is discussed in detail by Hamann.[5]

Making use of Eqs. (2.5), (2.12), and (2.13) and analytically continuing it to the real axis, we reduce Eq. (2.8) to the form

$$s_\uparrow(\omega+i\delta)=\rho\int d\omega'(\omega-\omega'+i\delta)^{-1}f(\omega')\times[1+\pi\rho\,\mathrm{Im}T_\downarrow(\omega'+i\delta)]. \tag{2.14}$$

Similarly, from Eq. (2.9) it follows that

$$s_\downarrow(\omega+i\delta)=\rho\int d\omega'(\omega-\omega'+i\delta)^{-1}[f(\omega')-1]\times[1+\pi\rho\,\mathrm{Im}T_\uparrow(\omega'+i\delta)]. \tag{2.15}$$

Finally the T matrices in Eqs. (2.14) and (2.15) are obtained from Eqs. (2.11) and (2.13):

$$T_{\uparrow,\downarrow}(\omega'+i\delta)=\Sigma_{\uparrow,\downarrow}(\omega'+i\delta)[1+i\pi\rho\Sigma_{\uparrow,\downarrow}(\omega'+i\delta)]^{-1}. \tag{2.16}$$

Equations (2.10) and (2.14)–(2.16) form a set of six coupled equations which we must now solve self-consistently.

III. SOLUTION OF THE COUPLED EQUATIONS

The equations for spin-up and spin-down quantities are coupled through Eqs. (2.14) and (2.15), but can be decoupled by using certain symmetry relations which we will now derive. The zeroth iteration, $s_\uparrow^0$, of Eq. (2.14) is obtained by taking $T=0$ on the right-hand side (and simply defines the bare s function). By changing the sign of the integration parameter ω' and making use of the identity $f(-\omega)=1-f(\omega)$ it is easily proved that

$$s_\uparrow^0(\omega+i\delta)=s_\downarrow^0(-\omega-i\delta)=s_\downarrow^{0*}(-\omega+i\delta). \tag{3.1}$$

Substituting this in Eqs. (2.10) and (2.16) yields the results

$$\Sigma_\uparrow^0(\omega+i\delta)=-\Sigma_\downarrow^{0*}(-\omega+i\delta), \tag{3.2}$$

$$T_\uparrow^0(\omega+i\delta)=-T_\downarrow^{0*}(-\omega+i\delta). \tag{3.3}$$

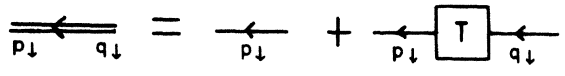

FIG. 2. Clothing of propagator expressed in terms of T matrix.

By using Eq. (3.3) in Eq. (2.14), one can prove that Eq. (3.1) also holds for the first iteration of $s_\uparrow$. In this way a cyclic procedure is generated by which Eqs. (3.1)–(3.3) can be proved for the nth-order iteration and these symmetry relations are therefore also satisfied by the exact self-consistent quantities.

The main purpose of this paper is a calculation of the resistivity R. According to Sec. IIC of paper I, this is given by

$$R/R_u = -\tfrac{1}{2}\pi\rho\,\mathrm{Im}[T_\uparrow(0+i\delta)+T_\downarrow(0+i\delta)]. \tag{3.4}$$

By using Eqs. (2.10) and (2.16) it can be shown that the right-hand side of Eq. (3.4) depends only on the quantities

$$\begin{aligned} &s_\uparrow(0+i\delta)+s_\downarrow(0+i\delta)=2\mathrm{Re}\,s_\uparrow(0+i\delta),\\ &s_\uparrow(0+i\delta)-s_\downarrow(0+i\delta)=2i\,\mathrm{Im}\,s_\uparrow(0+i\delta), \end{aligned} \tag{3.5}$$

where we have found the right-hand sides from Eq. (3.1). We now decouple the $S=\uparrow$ and $S=\downarrow$ equations by applying Eq. (3.1) to Eq. (2.15), and use of the identity $(x+i\delta)^{-1}\equiv P(x^{-1})-i\pi\delta(x)$ (where P is the principal part) yields

$$\mathrm{Re}\,s_\uparrow(0+i\delta)=\mathrm{Re}\,s_\uparrow^0(0+i\delta)+\pi\rho^2 \times P\int(d\omega/\omega)f(-\omega)\,\mathrm{Im}\,T_\uparrow(\omega+i\delta), \tag{3.6}$$

$$\mathrm{Im}s_\uparrow(0+i\delta)=-\tfrac{1}{2}\pi\rho\,[1+\pi\rho\,\mathrm{Im}\,T_\uparrow(0+i\delta)]. \tag{3.7}$$

As a result of the decoupling of the $S=\uparrow$ and $S=\downarrow$ equations, we are left with three complex equations to be solved simultaneously. One of these, Eq. (2.16), we eliminate by taking only the first term in its series expansion:

$$T_\uparrow(\omega+i\delta)\simeq\Sigma_\uparrow(\omega+i\delta). \tag{3.8}$$

Arguments to justify this approximation are given in Appendix B.

The factor $\mathrm{Im}\Sigma_\uparrow$ now needed in Eq. (3.7) is found from Eq. (2.10):

$$\pi\rho\,\mathrm{Im}\Sigma_\uparrow(0+i\delta)=y(x^2+y^2)^{-1}, \tag{3.9}$$

where we have introduced two new variables x and y defined by

$$\begin{aligned} &\pi\rho y=\mathrm{Im}s_\uparrow(0+i\delta),\\ &2\pi J\rho x=1+2J\,\mathrm{Re}s_\uparrow(0+i\delta). \end{aligned} \tag{3.10}$$

The zeroth-order approximation to these quantities are their bare values [see Eq. (B7) of paper I]

$$y^0=-\tfrac{1}{2},\quad x^0=(1/\pi)\ln(T_K/T). \tag{3.11}$$

By combining Eqs. (3.7)–(3.9) we find that x and y must satisfy the equation

$$2y^3+y^2+y\,(2x^2+1)+x^2=0. \tag{3.12}$$

This relation will be used later to calculate y, once x is known. At present we only state an approximate solution, obtained by use of Eq. (3.11) and Newton's iteration method:

$$y\simeq-\tfrac{1}{2}[1-(\tfrac{3}{2}+2x^2)^{-1}]. \tag{3.13}$$

It follows from Eq. (3.13) that we can expect $\mathrm{Im}s_\uparrow(0+i\delta)\simeq\mathrm{Im}s_\uparrow^0(0+i\delta)$ to be a good approximation for large x, i.e., $T\gg T_K$ or $T\ll T_K$, a fact which we use later on.

We now turn to the solution of Eq. (3.6). Here we make the approximation [see Eq. (2.14)]

$$\begin{aligned} \mathrm{Im}s_\uparrow(\omega+i\delta)&=-\pi\rho f(\omega)\,[1+\pi\rho\,\mathrm{Im}\,T_\uparrow(\omega+i\delta)]\\ &\simeq-\pi\rho f(\omega)=\mathrm{Im}s_\uparrow^0(\omega+i\delta). \end{aligned} \tag{3.14}$$

Using Eqs. (2.10), (3.8), and (3.14), Eq. (3.6) is then reduced to

$$\mathrm{Re}s_\uparrow(0+i\delta)=\mathrm{Re}s_\uparrow^0(0+i\delta) +\rho P\int\frac{-4J^2\pi^2\rho^2 f(\omega)f(-\omega)\,d\omega/\omega}{1+2J\mathrm{Re}s_\uparrow(\omega+i\delta)J^2+4J^2\pi^2\rho^2 f^2(\omega)}. \tag{3.15}$$

The approximation in Eq. (3.14) can now be justified as follows. First, the behavior of the integrand in Eq. (3.15) is dominated by the factor $f(\omega)f(-\omega)$, which at low temperatures is very sharply peaked near $\omega=0$ and zero elsewhere. This factor arises because $\mathrm{Im}s_\uparrow$ is proportional to $f(\omega)$—according to Eq. (3.14), a property of both the exact and approximate expressions.

Second, because of the peak mentioned above and which is enhanced by the ω in the denominator of the integrand, only the behavior of the integrand near $\omega=0$ is important and as pointed out below Eq. (3.13), the approximation can be expected to be good for $\omega=0$, at least far from T_K.

The peak in the integrand also justifies the approximation[10]

$$\mathrm{Re}s_\uparrow(\omega+i\delta)\simeq\mathrm{Re}s_\uparrow(0+i\delta) \tag{3.16}$$

in Eq. (3.15), which can then be rewritten by using Eqs. (3.10) and (3.11) as

$$\pi x+P\int_{-\infty}^{\infty}\frac{dz}{z}\left[\frac{F(z)F(-z)}{x^2+F^2(z)}\right]=\ln\left(\frac{T_K}{T}\right), \tag{3.17}$$

$$F(z)=(1+e^z)^{-1}.$$

From Eq. (3.11) it is clear that the principal-value integral, which we denote henceforth by $P(x)$, defines the correction to the non-self-consistent theory. In its corrected form, Eq. (3.17) is not amenable to a simple analytic solution any more. Note however, that its left-hand side is independent of temperature and the parameters of the physical system, so that x can still be expressed as a function of $\ln(T_K/T)$ only.

In Appendix C we use a contour integration to show that $P(x)$ can be expressed analytically in

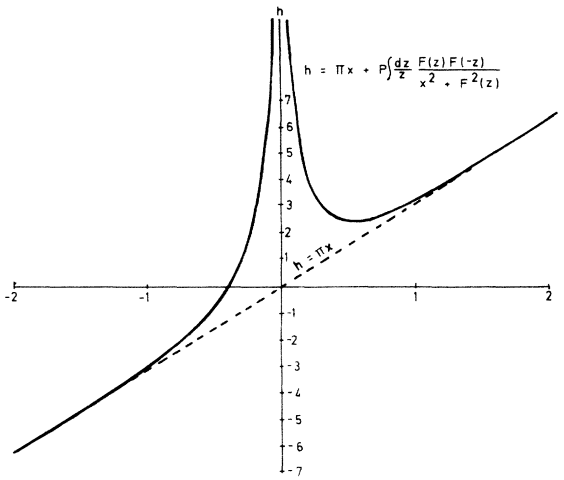

FIG. 3. Left-hand side of Eq. (3.17) as a function of x. The dashed line is the bare value.

terms of digamma functions. Its qualitative behavior, however, can be deduced directly from its integral representation in Eq. (3.17). Clearly it is an even function and $P(x) \to 0$ as $|x| \to \infty$. Even for $|x| \simeq 1$ the principal value is small because the function in square brackets represents a nearly symmetric peak around $z = 0$. For $x \to 0$, however, the function in square brackets approaches $F(-z)/F(z)$ and tends to infinity as $z \to \infty$. One can expect, therefore, that $P(x) \to \infty$ as $|x| \to 0$ but $P(x) \simeq 0$ elsewhere. This is borne out by the numerical plot of the left-hand side of Eq. (3.17), given in Fig. 3.

We can solve Eq. (3.17) graphically by finding, for each value of (T_K/T), the intersection of the horizontal line $h = \ln(T_K/T)$ with the curve in Fig. 3. At large values of T (i.e., $h \ll 0$) it is seen that this value of x coincides with the bare value x^0, found from the intersection with the dashed line. As the Kondo temperature T_K is approached, x deviates from x^0 and the value $x = 0$ is reached only when $T \to 0$. The importance of this fact is realized when it is recalled that in the bare version of the theory (see paper I) the resistivity reached a maximum at the Kondo temperature, i.e., for $x^0 = 0$. Consequently, even at this stage one can expect that the self-consistent resistivity will saturate at $T = 0$.

At a temperature below T_K, two additional solutions of Eq. (3.17) appear. One of these also tends to zero as $T \to 0$, and the other approaches the bare value.

Figure 4 represents a plot of values for x obtained by a numerical method similar to the graphical method outlined above. These values can then be substituted in Eq. (3.12) and a corresponding set of values obtained for y, also shown in Fig. 4.

Calculation of the resistivity. Having found x and y, which are essentially the real and imaginary parts of $s_1(0 + i\delta)$, we are now in a position to calculate the Kondo resistivity R from Eq. (3.4). The full T matrix can be used here, but numerically the result is very similar to the much simpler one derived by using its self-energy approximation [Eq. (3.8)]:

$$R/R_u = -y(x^2 + y^2)^{-1}. \tag{3.18}$$

This is essentially the same formula as the main result of paper I [Eq. (5.11)] but instead of their bare values, the self-consistently-calculated values for x and y are used. The resulting behavior of R as a function of T is illustrated by Fig. 5, while numerical values for use in fitting experimental data are given in Table I.

Comparison of Fig. 5 and Fig. 10 of paper I shows a marked difference between the clothed and bare versions of the theory. As predicted above, instead of vanishing the resistivity now saturates to a finite limit as $T \to 0$; and from Eqs. (3.12) and (3.18) it is easy to show that this limiting value (when both $x \to 0$ and $y \to 0$) is just the unitarity limit, R_u. This behavior corresponds at least qualitatively with experimental observations and with the Nagaoka-Hamann-Bloomfield theory[2-4] (also shown in Fig. 5). In Sec. IV we present a more detailed comparison with both of these. As shown in Fig. 5, a second branch appears on the resistivity graph at a temperature well below T_K. Without further investigation, we assume here that this branch has no physical significance because it cannot be reached in a continuous fashion when moving from high to low temperatures.

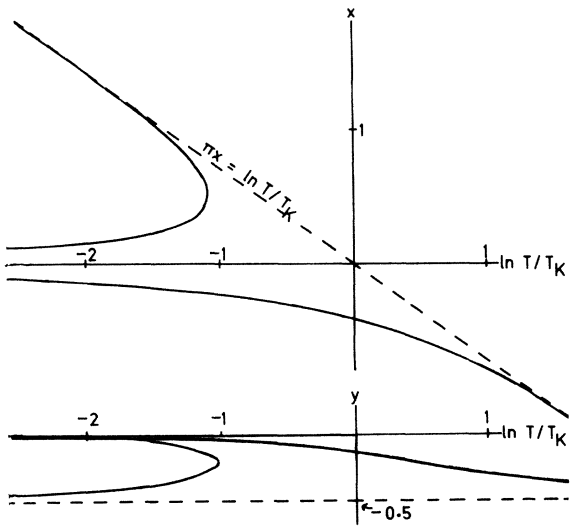

FIG. 4. Numerical results for x and y as functions of $\ln(T_K/T)$. Bare values x^0 and y^0 are indicated by dashed lines.

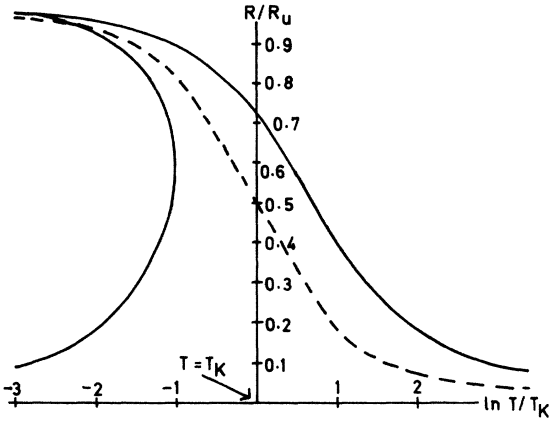

FIG. 5. Our selfconsistently calculated resistivity as a function of the reduced temperature, compared with the Hamann formula for $S=\frac{1}{2}$ (dashed line).

As a final remark we can now discuss the problem raised in Sec. I—how the inclusion of clothed diagrams in the self-energy sum can drastically alter the predicted behavior at $T=0$, even though they are of lower order in the logarithmic divergence at this point than the bare graphs. Referring to Fig. 3, we see that it is true that Eq. (3.17) which is satisfied by x is only significantly altered in the vicinity of $x=0$ (i.e., in "bare language," near T_K) and specifically, the bare solution remains valid for $x\to\infty$ (i.e., $T\to 0$). However, the structure of Eq. (3.17) is such that the deviation from the bare value at $x=0$ separates its solutions into two branches. While the bare solution which gives rise to a vanishing resistivity at $T=0$ remains valid mathematically, it is now located on a branch which can be ruled out on physical grounds.

IV. COMPARISON WITH EXPERIMENT

As a basis of comparison we choose the experimental data on *Cu*Cr(12 ppm) of Daybell and Steyert,[11] also used by Heeger[12] for comparison with the Hamann formula (see below).

In the work of Refs. 2–4, which leads to the Hamann formula, the magnitude S of the impurity spin is a free parameter. For a fair comparison with our results it must be restricted to $S=\frac{1}{2}$, and the Hamann formula [Eq. (16.2) of Ref. 12] becomes

$$R/R_u=\tfrac{1}{2}\{1-\ln(T/T_K)[\ln^2(T/T_K)+\tfrac{3}{4}\pi^2]^{-1/2}\}. \tag{4.1}$$

In both theories T_K is now the only free parameter, and when R is plotted as a function of $\ln T$ we can interpret $\ln T_K$ simply as a shift along the horizontal axis.

The data presented by Daybell and Steyert[11] are the resistivity values of the *Cu*Cr alloy after the pure-Cu resistivity has been subtracted. It still includes a background R_b due to the impurity potential, distortion of the crystal lattice, etc. which must be subtracted to leave the Kondo contribution due to spin-spin scattering. As a first approximation R_b is usually taken as a temperature-independent parameter, adjusted to give a good fit of the theory.

Even when taking the background into account, it is found that the experimental resistivity saturates to a considerably higher value than R_u [defined in Eq. (2.14) of paper I]. As pointed out by Heeger[12] the reason for this is that R_u also depends on S, and for $S=\frac{3}{2}$ the correct value is obtained. This problem is usually avoided by finding R_u from the data, i.e., after subtraction of R_b all values are divided by the zero-temperature value $R(0)$.

A much more serious discrepancy is the fact that (as seen from Fig. 5) for both the Hamann formula and our theory the saturation of R takes place over a range of $\simeq 6$ decades in the temperature, while typical experimental values range between 1 and 3 decades. Even if the high-temperature tail of the data is well fitted, the rise in resistivity will for this reason inevitably be too slow as $T\to 0$. This fact is illustrated by Fig. 6.

The parameters for fitting the Hamann formula are obtained as follows. From Eq. (4.1) it follows that $T=T_K$ defines the inflection point of the resistivity curve, and can be read off directly from Daybell and Steyert's plot of their data. The relation $R(T_K)=0.5$ can then be used to calculate R_b. For the *Cu*Cr system, Heeger[12] finds $T_K=2.2$ K and $R_b=8\ \mu\Omega$ cm/at.% which gives the curve[13] indicated in Fig. 6.

In our theory T_K has no such simple interpreta-

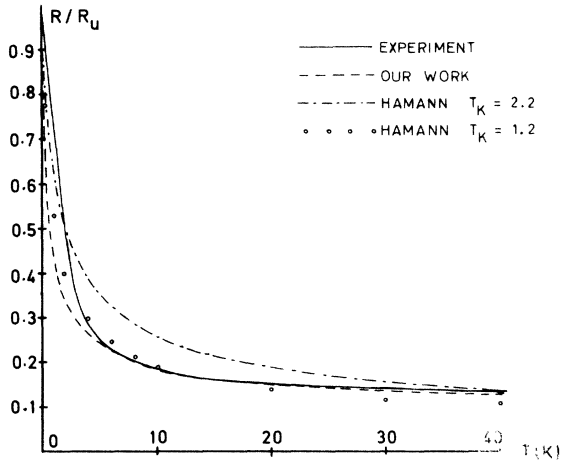

FIG. 6. Comparison of theoretical resistivity curves with the experimental values for *Cu*Cr (12 ppm) from Ref. 11.

tion, which complicates the determination of R_b. As its choice is regarded as rather arbitrary, we simply adopt Heeger's value and find T_K by shifting the theoretical curve along the horizontal axis to obtain the best fit. This yields the broken line in Fig. 6 which has $T_K = 0.125$ K.

It might be argued that our theory fits the data better than the Hamann formula because of the different procedure used. To test this, we have also fitted the Hamann formula without making use of the inflection point and find the curve indicated by the circles in Fig. 6, with $T_K = 1.2$ K. Comparison of the various curves in Fig. 6 justifies the conclusion that our theory gives a slightly better fit than the Hamann formula in the high-temperature region, while neither theory is adequate to explain the fast rise of the resistivity at low temperatures.

Despite their widely different appearances, it seems that numerically there is a close resemblance between our theory and the Nagaoka-Hamann-Bloomfield theory. In Appendix A we investigate this further by showing that Hamann's integral equation can be derived from our self-consistent equations by introducing a number of approximations.

ACKNOWLEDGMENT

The author wishes to express his sincere appreciation to Professor R. H. Lemmer for his encouragement and support of this work.

APPENDIX A: DERIVATION OF HAMANN'S INTEGRAL EQUATION

We investigate here the connection between our work and the Nagaoka-Hamann-Bloomfield theory[2-4] by indicating briefly how Hamann's integral equation (in the form given by Kondo[14]) can be derived from our results. The approximations that we make are labeled (A1)–(A7).

By comparing Eq. (2.16) of paper I with Eq. (18.15) of Ref. 14, it is seen that the function $t(\omega)$ in Hamann's work is essentially the same as our $T(\omega)$ obtained from Eq. (2.17) of paper I:

$$T(\omega) = \tfrac{1}{2}[T_\uparrow(\omega) + T_\downarrow(\omega)]$$

The following steps are involved in the derivation:

(i) Equation (2.16) is used to express T as a function of the sum $(\Sigma_\uparrow + \Sigma_\downarrow)$ and the product $(\Sigma_\uparrow\Sigma_\downarrow)$.

(ii) By means of Eq. (2.10) we find

$$\Sigma_\uparrow + \Sigma_\downarrow = 4J^2(s_\uparrow - s_\downarrow)[1 + 2J(s_\uparrow + s_\downarrow) + 4J^2 s_\uparrow s_\downarrow]^{-1}$$
$$\simeq 4J^2(s_\uparrow - s_\downarrow)[1 + 2J(s_\uparrow + s_\downarrow)]^{-1}. \quad \text{(A1)}$$

This is exactly the same approximation that was used in paper I to derive the non-self-consistent Nagaoka result. We can also express $\Sigma_\uparrow\Sigma_\downarrow$ in a quotient form, with the same denominator to which (A1) is also applied, and a numerator in which similarly only the term of lowest order in J is retained.

(iii) In the resulting expression for $T(\omega + i\delta)$ we use

$$s_\uparrow(\omega + i\delta) - s_\downarrow(\omega + i\delta) \simeq s_\uparrow(0 + i\delta) - s_\downarrow(0 + i\delta) \quad \text{(A2)}$$
$$\simeq -\pi\rho i. \quad \text{(A3)}$$

Equation (A3) is derived from Eqs. (3.5) and (3.7) by neglecting correction terms of order J^2 and higher.

(iv) In terms of Kondo's[14] parameter $b = 3J^2\pi^2\rho^2$ (in our notation) we find

$$i\pi\rho T = b[1 + 2J(s_\uparrow + s_\downarrow) + \tfrac{5}{3}b]^{-1}$$
$$\simeq b[1 + 2J(s_\uparrow + s_\downarrow) + b]^{-1}. \quad \text{(A4)}$$

In paper I it was seen that various approximations for the self-energy yield the same functional form for T, but that the coefficient of the additive constant b in the numerator is very sensitive to which subset of graphs is included. Consequently, we interpret approximation (A4) as an indication that the Nagaoka decoupling is equivalent to a sum, slightly different from our sum of parquet graphs.

(v) The sum $s_\uparrow + s_\downarrow$ is obtained from Eqs. (2.14) and (2.15):

$$s_\uparrow(\omega + i\delta) + s_\downarrow(\omega + i\delta) = \rho\int d\omega'\,(\omega - \omega' + i\delta)^{-1}[f(\omega') - \tfrac{1}{2}]$$
$$\times[1 + 2\pi\rho\,\mathrm{Im}T(\omega' + i\delta)].$$

Here we have used the approximation

$$\int d\omega'(\omega - \omega' + i\delta)\,[\mathrm{Im}T_\uparrow(\omega' + i\delta) - \mathrm{Im}T_\downarrow(\omega' + i\delta)] \simeq 0. \quad \text{(A5)}$$

(vi) Following Kondo,[14] we define

$$\Psi(\omega \pm i\delta) = 1 \mp 2\pi i\rho T(\omega + i\delta);$$

then

$$1 + 2\pi\rho\,\mathrm{Im}T(\omega' + i\delta) \simeq \Psi(\omega' - i\delta),$$

where we have used the identity $\mathrm{Im}T(\omega' + \delta) = -\mathrm{Im}T(\omega' - i\delta)$ and the approximation

$$\mathrm{Re}T(\omega' + i\delta) \simeq 0, \quad \text{(A6)}$$

which is exact for $\omega' = 0$.

(vii) Combining Eq. (A4) with these results, we find

$$\Psi(\omega' + i\delta) = \frac{1 - b + 2J\rho\int[f(\omega') - \tfrac{1}{2}]\Psi(\omega' - i\delta)\,d\omega'/(\omega - \omega' + i\delta)}{1 + b + 2J\rho\int[f(\omega') - \tfrac{1}{2}]\Psi(\omega' - i\delta)\,d\omega'/(\omega - \omega' + i\delta)},$$

which is essentially Hamann's integral equation [Eq. (18.26) of Ref. 14] if we make the final approximation

$$\Psi(\omega' - i\delta) \simeq 1 \quad \text{(A7)}$$

in the numerator.

We have shown that approximations (A1)–(A7) are sufficient for deriving the Hamann equation. Whether they are also necessary, and if so what the detailed justifications are, is not yet clear. Depending on this, two tentative conclusions can be made: (i) The Nagaoka decoupling is valid only for a weak interaction J [see (A1), (A3)]; (ii) the T matrix obtained from Hamann's equation is correct only for $\omega = 0$ [see (A2), (A6)].

APPENDIX B: JUSTIFICATION OF EQ. (3.8)

The approximation $T \simeq \Sigma$ of Eq. (3.8) is used twice in our work. In the first case, it is used to simplify the derivation of Eq. (3.12). If the full T matrix is used here, we find instead an equation of fifth order in y, but the final relation between y and temperature shows a behavior very similar to Fig. 4. As y does not make an important contribution in any case to the temperature dependence of R, the self-energy approximation is sufficiently accurate.

Equation (3.8) is also used to reduce Eq. (3.6) to Eq. (3.15). Our solution of Eq. (3.15) relies on the peaked behavior of the factor $f(\omega)f(-\omega)$ in the integrand, where $f(\omega)$ is contributed by the Σ approximation of T in Eq. (3.6). As seen from Eq. (2.16) the full T matrix is a power series in Σ, so that each term in its expansion is proportional to a power of $f(\omega)$. At low temperatures $f(\omega)$ is nearly a step function and $f^n(\omega) \simeq f(\omega)$. Consequently, a similar peaked behavior can be expected when the full T matrix is used in the integrand. This is confirmed by numerically calculating the integrand using the full non-self-consistent T matrix.

APPENDIX C: CALCULATION OF $P(x)$

Here we calculate the principal-value integral $P(x)$ defined in Eq. (3.17). Rewritten in terms of $\xi = 1/x$ it is given by

$$P(\xi) = \xi^2 P \int_{-\infty}^{\infty} e^{\varepsilon} [(1+e^{\varepsilon})^2 + \xi^2]^{-1} d\varepsilon / \varepsilon \,. \tag{C1}$$

For complex z, the integrand vanishes everywhere (except at the isolated point $\theta = \frac{\pi}{2}$) on the infinite half-circle in the upper half-plane. Consequently $P(\xi)$ can be evaluated by contour integration and we find

$$P(\xi) = 2\pi i \xi^2 \left(\tfrac{1}{2} r + \sum_n (r_n + r_n') \right) , \tag{C2}$$

where $r = (4+\xi^2)^{-1}$ is the residue of the integrand at $z = 0$, while r_n and r_n' are the residues at the double series of poles

$$z_n = \zeta + (2n+1)\pi i, \quad z_n' = \zeta^* + (2n+1)\pi i, \quad n = 0, 1, 2, \ldots \tag{C3}$$

and ζ is defined by the principal root of $e^{\zeta} = 1 + i\xi$. The residues are given by

$$r_n = \{ -2i\xi [\zeta + (2n+1)\pi i] \}^{-1}, \quad r_n' = \{ 2i\xi [\zeta^* + (2n+1)\pi i] \}^{-1} . \tag{C4}$$

After substituting the values of the residues, we reduce Eq. (C2) to

$$\frac{1}{\xi^2} P(\xi) = \frac{\pi i}{4+\xi^2} + \frac{\pi}{\xi} \left(2i \operatorname{Im} \sum_n \frac{\zeta^*}{\zeta^{*2} + (2n+1)^2 \pi^2} + 2\pi \operatorname{Im} \sum_n \frac{(2n+1)}{\zeta^{*2} + (2n+1)^2 \pi^2} \right) . \tag{C5}$$

The standard result

$$\tan(\tfrac{1}{2} z) = 4 \sum z [z^2 + (2n+1)^2 \pi^2]^{-1} \tag{C6}$$

is now used to cancel the first term in Eq. (C5) against the first sum, and the second sum is separated in partial fractions so that the final result is

$$P(\xi) = \tfrac{1}{2} \xi \operatorname{Im} [\psi(\tfrac{1}{2} + i\zeta/2\pi) + \psi(\tfrac{1}{2} - i\zeta/2\pi)] . \tag{C7}$$

Here $\psi(z)$ is the digamma function, defined for example in Abramowitz and Stegun.[15]

Asymptotic behavior as $\xi \to 0$. When $\xi \to 0$ it is seen that $\zeta \to 0$. By performing a Taylor expansion of the ψ functions in Eq. (C7) around $z = \frac{1}{2}$ it can be shown that $P(\xi) \to c\xi^4$ as $\xi \to 0$, where c is a constant.

The limit $\xi \to \infty$. Now $\zeta \to \ln|\xi| + i\pi/2$, and we have

$$\psi(\tfrac{1}{2} + i\zeta/2\pi) \to \psi(\tfrac{1}{4} + i \ln\xi/2\pi), \quad \psi(\tfrac{1}{2} - i\zeta/2\pi) \to \psi(\tfrac{3}{4} - i \ln\xi/2\pi) . \tag{C8}$$

The asymptotic formula [Eq. (6.3.18) of Ref. 15] $\psi(z) \sim \ln z - 1/2z$ and an addition formula for arctan [Eq. (4.4.34) of Ref. 15] is applied to Eqs. (C7) and (C8) to obtain the result

$$P(\xi) \sim \tfrac{1}{2}\pi \frac{\xi}{\ln\xi} + \frac{9\pi^3 \xi}{8 \ln^3 \xi} + \cdots . \tag{C9}$$

Finally, we transform back to our original variables to obtain

$$P(x) \to 0.2131\, x^{-4} \text{ as } x \to \infty, \quad P(x) \to -\tfrac{1}{2}\pi (x \ln x)^{-1} \text{ as } x \to 0 . \tag{C10}$$

This is, in quantitative form, the behavior discussed below Eq. (3.17).

---

*This work is based on a part of a Ph.D. thesis submitted by the author to the Physics Dept., Rand Afrikans University, Johannesburg (December 1972).

†Research supported by a bursary from the South African Council for Scientific and Industrial Research, Pretoria.

[1] W. S. Verwoerd, preceding paper, Phys. Rev. B 10, 2868

(1974).
[2]Y. Nagaoka, Phys. Rev. 138, A1112 (1965).
[3]D. R. Hamann, Phys. Rev. 158, 570 (1967).
[4]P. E. Bloomfield and D. R. Hamann, Phys. Rev. 164, 856 (1967).
[5]C. Y. Cheung and R. D. Mattuck, Phys. Rev. B 2, 2735 (1970).
[6]A. L. Fetter and J. D. Walecka, *Quantum Theory of Many-Particle Systems* (McGraw-Hill, New York, 1971).
[7]R. D. Mattuck, *A Guide to Feynman Diagrams in the Many-Body Problem* (McGraw-Hill, New York, 1967).
[8]J. Kondo, Prog. Theor. Phys. (Kyoto) 32, 37 (1964).
[9]This can be confirmed by explicitly drawing simple diagrams like $\Sigma_{1\uparrow}$ clothed with $\Sigma_{1\uparrow}$ and $\Sigma_{1\downarrow}$ respectively, in the Goldstone convention. It is seen that the first of these contains anomalous d lines and is therefore unacceptable (even at finite temperatures, see Sec. IV B of paper I).
[10]Near T_K [defined by $1+2J\mathrm{Re}s_\uparrow(0+i\delta)=0$] the peak can be expected to shift away from $\omega=0$, but for a realistic magnitude of (Jp) it can be shown that the shift is small. According to Eq. (2.14), $\mathrm{Re}s_\uparrow(\omega+i\delta)$ is a slowly varying function of ω because it is only connected through a principal-value integral. Consequently Eq. (3.16) holds even at T_K.
[11]M. D. Daybell and W. A. Steyert, Phys. Rev. Lett. 20, 195 (1968).
[12]A. J. Heeger, Solid State Phys. 23, 283 (1969).
[13]A better fit is often obtained in the literature by using a small values of S [for example $S=0.11$ in the work of M. Dietrich and W. Gey, Solid State Commun. 11, 655 (1972)]. This is successful because for the Hamann formula the rise at low temperatures becomes steeper with decreasing S. However, as pointed out above, S should be determined from the values of R_u and this tends to give much larger values.
[14]J. Kondo, Solid State Phys. 23, 244 (1969).
[15]M. Abramowitz and I. Stegun, *Handbook of Mathematical Functions* (Dover, New York, 1965).